On the Microstructure-Polarization Behavior Correlation of a 9Cr-1Mo Steel Weld Joint

G. George, H. Shaikh, N. Parvathavarthini, R.P. George, and H.S. Khatak

(Submitted 9 November 2000)

The use of 9Cr-1Mo ferritic steel necessitates its fabrication by the process of welding. The heat-affected zone (HAZ) of 9Cr-1Mo ferritic steel is a combination of many microstructures. In the present study, the corrosion properties of the base metal, weld metal, and the various regions of the HAZ are assessed with respect to their microstructures. The various microstructures in the HAZ were simulated by heat treatment of the normalized and tempered base metal at 1463, 1200, and 1138 K for 5 min followed by oil quenching. The microstructure of the base metal in the normalized and tempered condition revealed martensite laths with $M_{23}C_6$ carbides at lath boundaries, and uniform dispersion of fine, acicular M_2C. The weld metal showed predominantly martensitic structure with dispersion of carbides. Simulation of the microstructures of the HAZ by heat treatment resulted in the following microstructures: coarse-grained martensite of 75 μm size at 1463 K, fine-grained martensite at 1200 K, and martensite + proeutectoid α-ferrite at 1138 K. In all cases, carbide precipitation was observed in the martensitic matrix. Microhardness measurements of HAZ-simulated base metal showed increasing hardness with increasing heat treatment temperature. The hardness values obtained corresponded very well with the regions of the actual HAZ in the weld joint. Electrochemical polarization studies were carried out on the base metal, weld metal, weldment (base metal + weld metal + HAZ), and the simulated HAZ structures in 0.5 M sulfuric acid solution. Critical current densities (i_{crit1} and i_{crit2}), passive current densities (i_{pass} and $i_{sec\text{-}pass}$), and transpassive potential (E_{tp}) were the parameters considered for evaluating the corrosion resistance. The HAZ structures simulated at 1463 and 1200 K, corresponding to coarse- and fine-grained martensitic regions of an actual HAZ, had corrosion properties as good as the normalized and tempered base metal. Of the various simulated HAZ structures, the intercritical region, which was simulated at 1138 K, possessed the worst corrosion resistance. The weld metal possessed the worst corrosion resistance of the various microstructural regions in the weld joint. The weldment adopted the degraded corrosion properties of the weld metal.

Keywords coarse-grained martensite, fine-grained martensite, intercritical region, polarization behavior, transpassive potential

Introduction

Chromium-molybdenum steels are widely used in the power and process industries, combining high strengths at both ambient and high temperatures with adequate toughness. The availability of these properties in low alloy steels makes them economically attractive. These steels contain chromium contents up to 12% with usually about 1% Mo. The requirements of these steels with high Cr content has been necessitated for high-temperature operation in corrosive environments such as those of the nuclear and petrochemical industries.[1,2] The properties are controlled by microstructure, which, in turn, depends on the heat treatment. The heat treatments given are also simple and therefore, economically viable. The steels most commonly used vary in chromium content from 0.5 to 12% and all of them contain some molybdenum, usually up to a maximum of 1%. In recent years, 9Cr-1Mo steel has become a favored tubing material for fast reactor steam generators because of its low thermal expansion, high resistance to chloride-induced stress corrosion cracking, acceptable mechanical properties at service temperatures, and easy control of microstructure.[3] The material undergoes degradation in properties due to long-term exposures to elevated temperatures and to aggressive environments. It is also susceptible to intergranular stress corrosion cracking in environments where hydrogen is produced.[4–7] The use of these steels necessitates their joining by welding. These steels are readily weldable only if recommended welding practices such as preheating and postweld heating are followed, failing which a host of cracking problems,[8] such as delayed cracking, hot cracking and reheat cracking, and sensitization,[9] could result. The failure of a ferritic steel component is initiated during welding or during service in a localized microscopic region of the weldment.[10] This is due to the significant differences in the behavior of the various regions of the weldment because of the heterogeneity in their microstructure.[11,12] The variations in the microstructure and microchemistry of the different regions in ferritic steel weldment arise due to the differences in the thermal cycles experienced by these regions.[8] The major causes for failure of ferritic steel weldments have been identified to be delta-ferrite formation, impurity elements segregation, overcoarsening of austenite near the weld metal, and formation of intercritical region.[10,13–16] In addition, sensitization, and as a result intergranular corrosion, has been reported under certain conditions such as improper postweld heat treatment.

Although 9Cr-1Mo steel is used in the normalized and tempered condition, sharp changes occur in the microstructure of

G. George, H. Shaikh, N. Parvathavarthini, R.P. George, and **H.S. Khatak,** Corrosion Science and Technology Division, Indira Gandhi Centre for Atomic Research, Kalpakkm - 603 102, Tamil Nadu, India. Contact e-mail: khatak@igcar.ernet.in.

Table 1 Chemical compositions (wt.%) of base and weld metals of 9Cr-1Mo ferritic steel

Element	Cr	Mo	Mn	Ni	Si	C	P	S
Base metal	8.6	0.97	0.47	0.17	0.51	0.125	0.008	0.003
Weld metal	9.1	1.0	0.84	0.24	0.35	0.10	0.02	0.007

the weldment depending on the welding parameters. Metallurgical changes that occur during welding are consequent to the wide range of heating and cooling cycles experienced by different regions of the weldment. The essential differences in microstructures arise in terms of the carbides present in the weld metal, heat-affected zone (HAZ), and parent metal.[17]

Not much work has been reported on the effect of heat treatment and microstructure on the aqueous corrosion behavior of 9Cr-1Mo steel.[18–21] These steels show a characteristic active-passive behavior in a 0.5 M H_2SO_4 solution with and without arsenic additions.[18] No active-passive behavior was observed in this steel in a sulfuric acid medium containing chloride ion.[21] The flade potential, critical current density, and passive current density are higher when the microstructure contains proeutectoid ferrite and carbides as compared to that which contains a single martensite phase.[18] Decreasing the cooling rate decreased the pitting corrosion resistance (PCR) of the steel during the early stages of tempering. The PCR was restored thereafter.[18] Modified 9Cr-1Mo steel showed better corrosion resistance than the normal variety in sulfuric acid and sea water environments.[19]

Reports on the corrosion behavior of weldments of 9Cr-1Mo are few and far between. Available reports suggest that the high-temperature oxidation resistance of various regions of 9Cr-1Mo weldments increases in the order weld metal, HAZ, and base metal;[22] while in 2.25Cr-1Mo steel, the HAZ has the least oxidation resistance followed by the weld metal and base metal.[23] However, such authentic reports on the aqueous corrosion behavior of the various regions of the weldment, separately and as a whole, are not available in the literature.

Keeping the above observations in mind, the present study was designed to correlate the microstructures of the various regions in a weld joint of 9Cr-1Mo ferritic steel to their electrochemical polarization behavior. The various regions of the HAZ were simulated by heat treatment.

Experimental Procedures

V-groove joints of 9Cr-1Mo ferritic steel were multipass welded using the manual metal arc welding process (chemical composition of base and weld metals are listed in Table 1). Samples for polarization studies were cut from the base metal, weld metal (center of the fusion zone), and weldment. The various microstructures encountered in the HAZ were simulated by heat treatment of the normalized and tempered base metal. The temperature and time of simulation heat treatments, *viz.* 1463, 1200, and 1183 K, were selected based on prior experience in our laboratory.[24] After isothermal heating, the samples were quenched in oil.

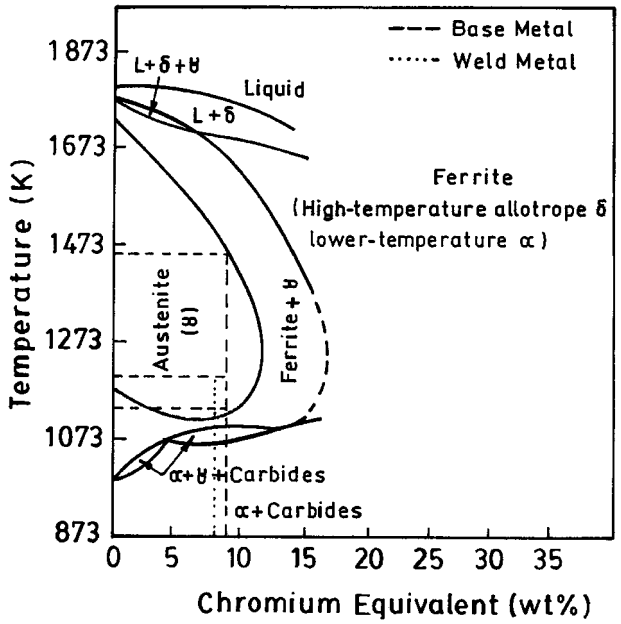

Fig. 1 Pseudoequilibrium diagram showing the dependence of the existence of various phases on chromium equivalent. The base and weld metals of the present study are located on the diagram

Optical microscopic examination of the base and weld metals, weldments, and simulated HAZ samples were carried out using an optical microscope after etching them in hot Vilella's reagent (1 g picric acid, 5 mL concentrated HCl, and 100 mL ethanol or methanol) for 30 to 40 s. Grain size measurements were also carried out for the base metal and the different simulated HAZ structures.

Potentiodynamic polarization experiments were carried out on base and weld metals, weldments, and simulated HAZ samples in 0.5 M H_2SO_4. The electrolyte was taken in the standard polarization cell and was deaerated by purging oxygen-free dry argon gas for 60 min. Then, the specimen was immersed in the test solution for 60 min with argon gas bubbling through the solution during this period as well as during subsequent polarization test. The open circuit potential (OCP) of the specimen was measured against a saturated calomel electrode and was found to be quite stable within ± 1 mV. The anodic polarization tests were carried out at a scan rate of 10 mV/min from OCP to 1800 mV using a Wenking potentioscan model POS 73.

Results and Discussions

Addition of Cr to a steel, which is described by an iron-carbon system, improves the corrosion resistance due to the formation of a protective surface oxide film. Hence, the chromium equivalent of the alloy would play a significant role in microstructural control and thus affect the mechanical and corrosion properties. The pseudo-equilibrium diagram for the Fe-Cr-0.1% C system is given in Fig. 1.[25] The phase fields crossed during heating or cooling by a particular alloy are dependent on the chemical composition, which in turn can be expressed as the net chromium equivalent.[26] Patriarca *et al.*[26]

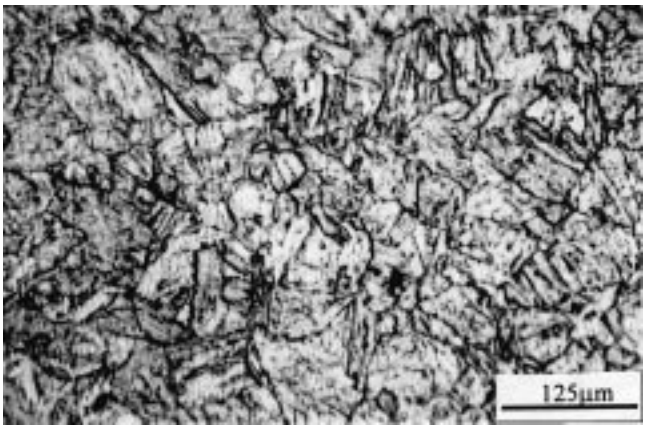

Fig. 2 Microstructure of 9Cr-1Mo ferritic steel base metal

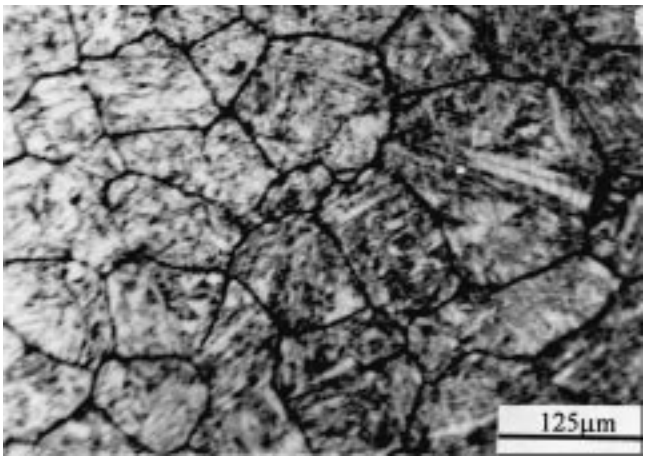

Fig. 3 Microstructure of the weld metal of 9Cr-1Mo ferritic steel

proposed a net chromium equivalent (NCE), which is expressed as

$$\begin{aligned}\text{NCE} = {} & \%\text{Cr} + 6 * \%\text{Si} + 4 * \%\text{Mo} + 1.5 * \%\text{W} \\ & + 11 * \%\text{V} + 5 * \%\text{Nb} + 12 * \%\text{Al} + 8 * \%\text{Ti} \\ & - 40 * \%\text{C} - 2 * \%\text{Mn} - 4 * \%\text{Ni} - 2 * \%\text{Co} \\ & - 30 * \%\text{N} - \%\text{Cu}\end{aligned}$$

For the alloy under investigation, the base metal had a NCE of 8.98, while the weld metal had a NCE of 8.56. For these values of NCE, the various regions of HAZ in the weldment and the various simulated HAZ structures are well within the austenite phase field. The solutionizing temperature for this alloy has been reported to be greater than 1273 K.[18] This would mean that, during welding, some regions of the HAZ and simulated HAZ structures of 1138 and 1200 K heat treatments would not see solutionizing temperatures and hence undissolved $M_{23}C_6$ carbides would be expected to be present in the microstructure.

Figure 2 shows the microstructure of the normalized and tempered base metal of 9Cr-1Mo steel. The structure of this base metal is reported to contain martensite laths with $M_{23}C_6$ carbides at lath boundaries, and uniform dispersion of fine, acicular M_2X, where X could be carbide or nitride, within the ferrite.[27] Figure 3 shows the microstructure of the weld metal of 9Cr-1Mo ferritic steel. The structure should have shown the presence of only the martensite phase.[28] This would have been the case with the microstructure of the top pass. However, since the weld metal was prepared by multipass welding, the martensite in the previous beads would have been tempered, leading to the precipitation of ferrite and carbide phases. Vijayalakshmi *et al.*[28] had reported the presence of prior austenite grains elongated in the direction of cooling. However, no such elongated grains were present in the weld metal of the present study. This could be attributed to the tempering effects on previous passes during multipass welding. Hence, the weld metal showed a structure similar to the base metal. The solidification of the liquid metal could proceed by two different routes depending on the chemical composition and the cooling rate: either 100% austenite, which subsequently could undergo a solid-state transformation to martensite, or a mixture of austenite with small amounts of delta-ferrite.[28] In the present study, no delta-ferrite was observed. This was because of the low NCE of the weld metal of 8.56. Vijayalakshmi *et al.*[28] also reported the absence of delta-ferrite in the weld metal of their study; while Laha,[29] Harries,[30] and Buchamyr *et al.*[31] reported the presence of delta-ferrite in the weld metal. Solidification of the liquid metal into the duplex $\delta + \gamma$ phase field has been reported in a series of steels with Cr content in the range of 9 to 12%, with 9% being the border line.[32] Apart from the cooling rate, which is governed by the thickness of the weld section, and the degree of repartitioning of Cr into the liquid, the solidification of 9Cr-1Mo steel into the duplex phase field depends critically on the amount of ferrite stabilizers, particularly, Si.[28] Though the amount of Si in the weld metal was 0.47%, the carbon content of the weld metal was 0.14%, which could cause the duplex $\delta + \gamma$ phase field to shift to higher Cr contents. Comparison of Fig. 2 and 3 indicates that the weld metal has a large grain size as compared to the base metal. This could be attributed to the higher temperatures that the multipass weld metal experiences during welding and also the longer times spent by the weld metal in the austenitizing temperature range during cooling of the weld metal.

The four main HAZ microstructures observed in the 9Cr-1Mo weld joint mainly depend on the peak temperatures attained in the different regions during welding.[13,33] The region closest to the fusion boundary experiences peak temperatures above AC_4 (boundary between γ and $\gamma + \delta$ fields). At this temperature, Laha *et al.*[24] reported the formation of δ-ferrite along the austenite grain boundaries. The resultant structure is coarse-grained martensite with delta-ferrite. They reported an austenitic grain size of about 80 m. This region was not obtained in the ferritic steel weldment of our study. This could be attributed to a NCE of 8.98 for the base metal. After this region, where the peak temperatures experienced by HAZ lie between AC_3 and AC_4, the carbides, which impede grain growth, dissolve. Saroja *et al.*[34] had reported that total solutionizing of the microstructure occurs above 1323 K. Laha *et al.*[24] reported an austenite grain size of about 60 m in this region. On cooling, this region would transform to coarse-grained martensite. The grain size decreases with increasing distance from the fusion

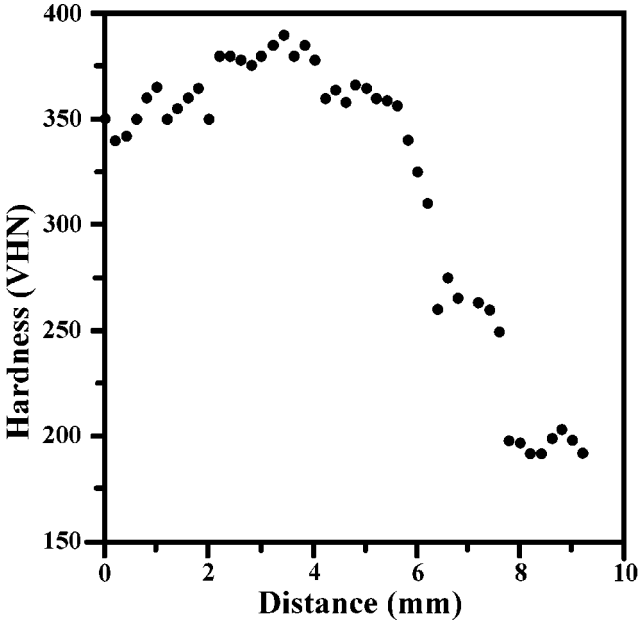

Fig. 4 Variation in microhardness across the various regions of the weld joint of 9Cr-1Mo ferritic steel

line as the peak temperature experienced decreases.[13,35] This would result in the formation of fine-grained martensite. When the HAZ experiences a peak temperature between AC_1 and AC_3, only partial transformation to austenite takes place. Consequently, the microstructure resulting after cooling would be a mixture of austenite transformed products surrounding the volumes of nontransformed ferrite, which would have been tempered during the thermal cycle. This region is known as the intercrtitical region.

Figure 4 gives the variation of microhardness across the weldment, starting from the weld metal. The first two millimeters of the graph replicate the hardness of the weld metal. The hardness of the weld metal is around 360 VHN. This low value of hardness could be because of the softening of the microstructure by multiple tempering as a result of multipass welding. Also, the large grain size of the weld metal could have contributed to its lower hardness. Figure 4 shows three distinct regions of hardness in the HAZ: (1) regions very adjacent to the weld zone, *i.e.*, those of coarse-grained martensite, having hardness of about 390 VHN; (2) regions containing fine-grained martensite having hardness of about 350 VHN; and (3) regions of low hardness of about 240 VHN. Trial simulations were carried out by aging the normalized and tempered base metal at 1463, 1200, and 1138 K for 5, 10, and 15 min; and then, based on comparison of microhardness values of these simulated structures and the actual HAZ structures, the time periods of ageing for simulation of HAZ structures were selected as 5 min at each of the above temperatures. Oil quenching was resorted to for simulation purposes. This was because the presence of metallic paths for heat conduction, due to thermal gradients across the weld joint, results in higher cooling rates than those attained during air cooling. The cooling rates attained in air equal 2 K/s, while those in water equal 100 K/s.[34] Hence, for simulation of HAZ structures, a cooling

Table 2 Microhardness and grain sizes of various HAZ-simulated structures

Temperature (K)	Time (min)	Grain size (μm)	Hardness (VHN)
Base metal	…	25	195
1138	5	27	253
1200	5	29	360
1463	5	77	390

rate greater than 2 K/s was desired. This was attained by using oil as a cooling medium in which the cooling rates attained were 20 K/s.[34] The hardness values and grain sizes of the various regions of the simulated HAZ structures are listed in Table 2. It is seen that the microhardness of the simulated HAZ microstructures matched very well with the actual values of the various regions of the HAZ. The HAZ-simulated microstructures are shown in Fig. 5(a) to (c). The simulated coarse-grained martensite regions are shown in Fig. 5(a). The coarse-grained martensite region has a higher hardness in spite of large grain size. This was because this region experienced temperatures beyond 1323 K, which resulted in total dissolution of all the carbides. This would increase solid solution strengthening as well as lead to formation of finer martensite due to depression of the M_s temperature.[36] The simulated region of fine-grained martensite is shown in Fig. 5(b). The fine-grained martensite region showed a slightly lower hardness than the coarse-grained martensite. This could be due to the region seeing temperatures below 1323 K. It is probable that all the carbides might not have gone into solid solution. This could result in a lesser effect of solid solution strengthening. Also, the range of temperatures over which the region cooled was lower, resulting in the formation of coarser martensite. A simulated intercritical region is shown in Fig. 5(c). The lower hardness of the intercritical region could be explained based on the presence of large amounts of proeutectoid ferrite.

The anodic polarization curves for the base metal, weld metal, three simulated HAZ structures, and the weldment of 9Cr-1Mo ferritic steel in 0.5 M H_2SO_4 solution at room temperature are shown in Fig. 6(a) to (f), respectively. All the specimens showed two peaks of active dissolution, primary passivity, secondary passivity, and transpassivity. The two peaks of active dissolution, nomenclatured as i_{crit1} and i_{crit2}, occur due to dissolution of Fe, Cr, and Mo. The corrosion products formed at i_{crit1} due to dissolution of these elements tend to passivate the material because an initial dip in the current density is observed. However, these products dissolve almost immediately and current density rises again to the value of i_{crit2}. The assessment of the polarization behavior was based on the following parameters, which are depicted in Fig. 6(a): critical current densities, i_{crit1} and i_{crit2}; primary passive current density, i_{pass}; secondary passive current density, $i_{sec\text{-}pass}$; primary passivation range, E_{pr1}; secondary passivation range, E_{pr2}; and transpassive potential, E_{tp}. The values of these parameters are listed in Table 3.

The results clearly show that the base metal, which is in the normalized and tempered condition, and simulated HAZ microstructures corresponding to 1200 and 1463 K heat treatments have values of i_{crit1}, i_{crit2}, i_{pass}, and $i_{sec\text{-}pass}$ that are sufficiently low—the only exception being the value of i_{crit2} for the

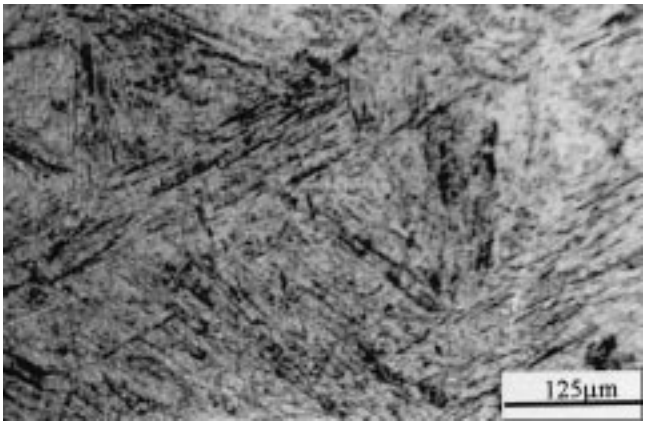

(**a**)

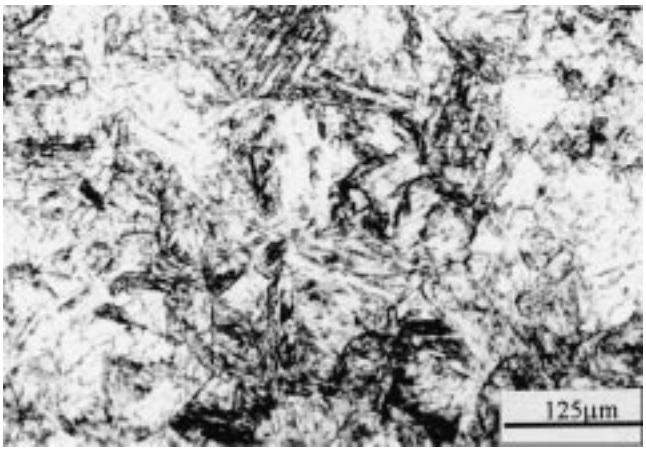

(**b**)

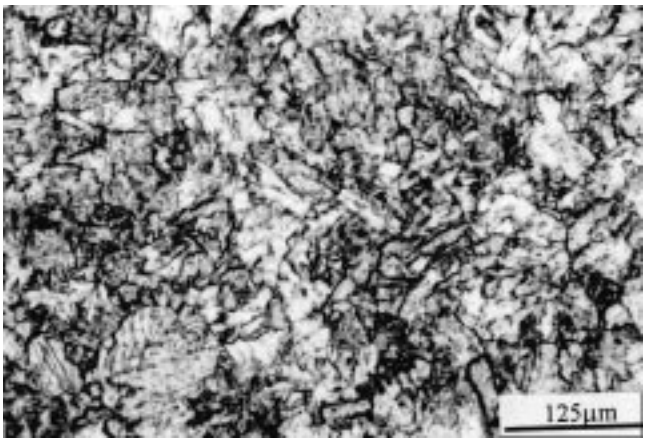

(**c**)

Fig. 5 Microstructures of the various regions of the HAZ simulated by heat treatment: (**a**) 1138 K, (**b**) 1200 K, and (**c**) 1463 K

base metal. The HAZ-simulated structure at 1138 K showed values of the above parameters that were nearly 2 times those of the base metal. The weld metal and weldment showed values that ranged between 2 and 3 times for the above parameters vis-à-vis the base metal. Of the entire gamut of structures investigated, the weldment showed the highest values of the above four parameters. Except for i_{crit2}, which was twice that of the weld metal, the values of other parameters of the weldment were close to that of the weld metal. The parameters i_{crit1} and i_{crit2} are a measure of the general corrosion rate of the material. The parameter i_{crit2} also depicts the maximum current density that the material acquires before attaining passivity. Higher values of i_{crit2} would mean that higher amounts of material would have to dissolve before the passivity of the material is attained. The passivity attained by the ferritic steels is due to formation of corrosion products on the surface. The passive films thus formed are not protective in nature as are those formed on the surfaces of stainless steels. The occurrence of primary passivity in ferritic steels was attributed to the formation of chromium hydroxide, $Cr(OH)_3$, or hydrated chromium oxide, $CrO_3 \cdot nH_2O$, while secondary passivity occurred due to the formation of iron oxide in 9Cr-1Mo steel in the H_2SO_4 medium.[20] Higher values of i_{crit2} suggest that a greater amount of material would have to dissolve to obtain the critical amounts of chromium hydroxide necessary for the material to become passive. In the case of the base metal and HAZ structures, there is a one-to-one correlation between i_{crit2} and the passivation current densities i_{pass} and $i_{sec\text{-}pass}$. Higher values of i_{crit2} resulted in higher values of i_{pass} and $i_{sec\text{-}pass}$. The values of i_{pass} and $i_{sec\text{-}pass}$ were at least 4 to 10 times higher for the weld metal and weldment as compared to the corresponding values for the base metal and HAZ structures. This could be attributed to the high concentration of microstructural defects in the weld metal, which made its passivation difficult. Correlation of the values of the various current densities with the various microstructures available in the 9Cr-1Mo ferritic steel weld joint showed that, from the point of view of general corrosion and passivity, the microstructures could be arranged in the following order of decreasing resistance: fine-grained martensite = coarse-grained martensite > tempered martensite + carbides microstructure of the normalized and tempered base metal ≫ martensite + proeutectoid ferrite + carbide microstructure of the intercritical region ≫ tempered martensite + carbide microstructure of the weld metal. These trends are on expected lines except for the results of the weld metal. Parvathavarthini *et al.*[18] had reported lower values of i_{crit} for single-phase martensitic structures with traces of $M_{23}C_6$ precipitates. In the weld metal, the single-phase microstructure is not the only criterion that governs the corrosion resistance. Residual stresses and a high density of metallurgical defects, such as dislocations, are present in weld metals. These would have significantly contributed to the higher corrosion susceptibility of the weld metal.

Analysis of the data on the range of passive potentials, E_{pr1} and E_{pr2}, did not show a systematic dependence on microstructure. The values of the passive potentials ranged between 475 and 650 mV. In all the heat-treated conditions, the transpassive potential, E_{tp}, was observed at sufficiently positive potentials where the protective, insoluble oxide film changed to a higher valency oxide which was soluble under the given condition and had no passivating properties. In this region, there is a transition from the formation of trivalent Cr to the formation of hexavalent Cr by the reaction

$$2Cr^{+3} + 7H_2O \rightarrow Cr_2O_7^{-2} + 14H^+ + 6e^{-}\text{[37]}$$

Higher values of transpassive potential, E_{tp}, would mean

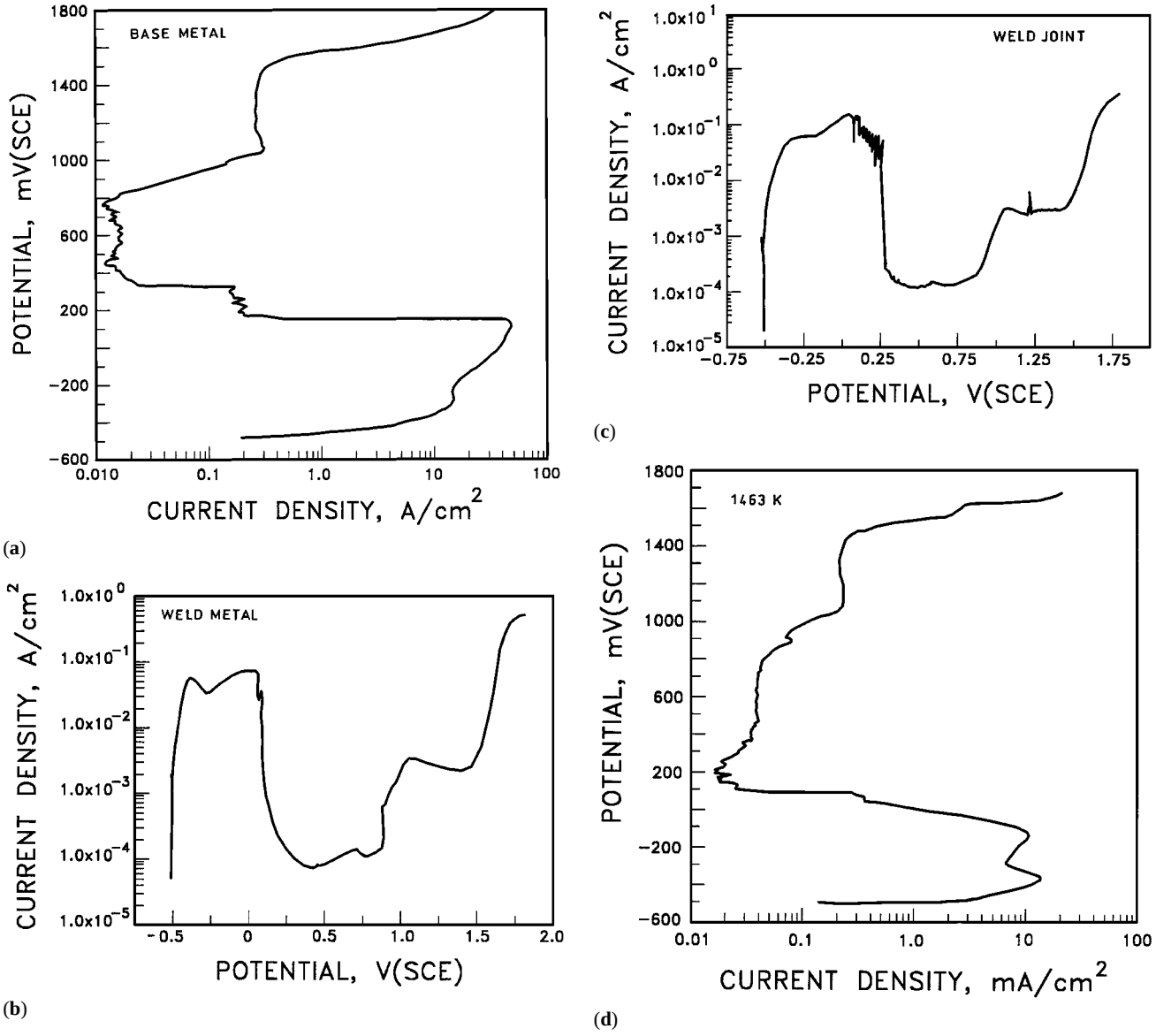

Fig. 6 Polarization curves in 0.5 M sulfuric acid for (**a**) base metal, (**b**) weld metal, and (**c**) weldment; the HAZ simulated by heat treatment: (**d**) 1463 K, (**e**) 1200 K, and (**f**) 1138 K

difficulty in breaking the passivity of the steel. The values of E_{tp} were the highest for normalized and tempered base metal. This could be attributed to the uniformity of the chemical composition that was attained during tempering. The E_{tp} value of the base metal was closely followed by the simulated structures of fine- and coarse-grained martensites. The lower E_{tp} value of the weld metal, vis-à-vis the normalized and tempered base metal, could be attributed to the high density of microsructural defects that are present in the former. The simulated intercritical microstructure possessed the lowest value of E_{tp}. This is understandable from the point of view of multiphase microstructure in the intercritical region. The weldment had a value of E_{tp}, which was close to the weld metal.

Ranking all the microstructures with the various parameters of assessment of corrosion, *viz.* i_{crit1}, i_{crit2}, i_{pass}, $i_{sec\text{-}pass}$, and E_{tp}, a microstructural correlation could be made as follows in decreasing order of overall corrosion resistance: fine-grained martensite, coarse-grained martensite (both simulated HAZ structures), tempered martensite + carbide microstructure of the normalized and tempered base metal ≫ martensite + proeutectoid ferrite + carbide microstructure of the intercritical region ≫ tempered martensite + carbide microstructure of the weld metal. The fact that the weldment acquired the corrosion properties of the weld metal suggests that the region with the worst corrosion properties governed the corrosion of the weld joint. This was confirmed by the visual observation of the anodically polarized weldment, which showed extensive dissolution of its weld metal component. This observation was in agreement with our studies on corrosion behavior of weld joints of nitrogen-added AISI type 316 L stainless steel, wherein the weldment adopted the corrosion properties of the worst component, *i.e.*, the base metal.[38]

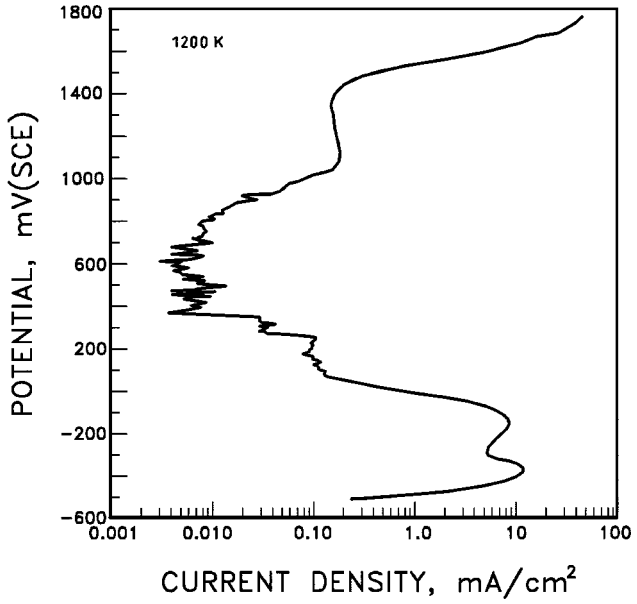

(**e**)

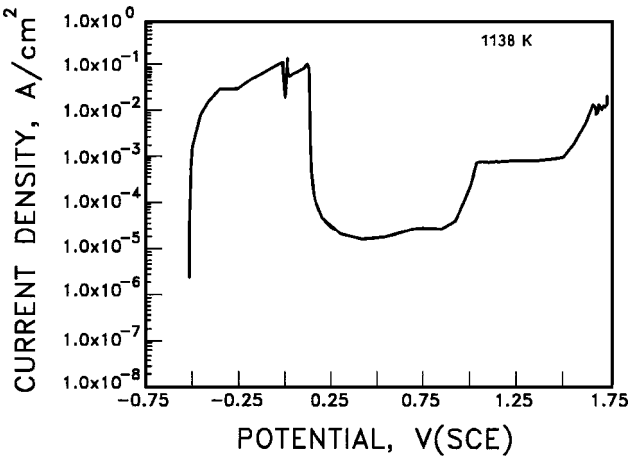

(**f**)

Fig. 6 Continued. Polarization curves in 0.5 M sulfuric acid for (**a**) base metal, (**b**) weld metal, and (**c**) weldment; the HAZ simulated by heat treatment: (**d**) 1463 K, (**e**) 1200 K, and (**f**) 1138 K

Table 3 Results of the electrochemical polarization studies on base metal, weld metal, weldment, and simulated heat-affected zone structures of 9Cr-1Mo steel

Material condition	i_{crit1} mA/cm^2	i_{crit2} mA/cm^2	i_{pass} mA/cm^2	$i_{sec\text{-}pass}$ mA/cm^2	E_{pr1} mV	E_{pr2} mV	E_{tp} mV
Base metal	15.8	52.0	0.013	0.3	606	615	1386
1138 K	28.7	109.0	0.022	0.7	508	475	1108
1200 K	11.8	8.6	0.004	0.182	574	595	1344
1463 K	13.9	10.3	0.015	0.219	586	600	1357
Weld metal	54.9	71.5	0.1	2.3	646	565	1308
Weldment	60.8	141.8	0.12	2.6	547	446	1267

Conclusions

The present study on the correlation of electrochemical polarization behavior in 0.5 M sulfuric acid, of the various regions of weld joints of 9Cr-1Mo steel with their microstructures, led to the following conclusions.

- HAZ structures simulated at 1463 and 1200 K, corresponding to coarse- and fine-grained martensitic regions of an actual HAZ, had corrosion properties as good as the normalized and tempered base metal.
- Of the various simulated HAZ structures, the intercritical region, which was simulated at 1138 K, possessed the worst corrosion resistance.
- The weld metal possessed the worst corrosion resistance of the various microstructural regions in the weld joint.
- The weldment adopted the degraded corrosion properties of the weld joint.

Acknowledgments

The authors acknowledge the help rendered by Mrs. K. Parimala of this laboratory in the experimental work. They also thank Drs. R.K. Dayal and P. Muraleedharan for their valuable discussions.

References

1. J.A.G. Holmes: *Nucl. Eng.,* 1981, vol. 23, p. 23.
2. F. Pollard: *Proc. ASM Int. Conf. on Production, Fabrication, Properties and Applications of Ferritic Steels for High Temperature Applications,* A.K. Khare, ed., ASM, Materials Park, OH, 1981, p. 153.
3. J. Orr and S.J. Sanderson: *Proc. Tropical Conf. on Ferritic Alloys for Use in Nuclear Energy Technologies,* Snowbird, UT, J.W. Davis and D.J. Michael, eds., TMS-AIME, Warrendale, PA, 1984, p. 261.
4. C.A. Hippsley and N.P. Haworth: *Mater. Sci. Technol.,* 1988, vol. 4, p. 791.
5. H. Kurahashi, T. Kurisu, Y. Sone, K. Wada, and Y. Nakai: *Corrosion/84,* NACE, Houston, TX, 1984, paper no. 212.
6. S.K. Banerji, C.J. McMohan, Jr., and H.C. Feng: *Metall. Trans. A,* 1978, vol. 9A, p. 237.
7. S.K. Banerji, C.L. Briant, and C.J. McMohan, Jr.: *Proc. Conf. on*

Environment Sensitive Cracking of Materials, The Metals Society, London, 1977, p. 437.
8. R. Menon and K.K. Khan: "A Report on Transformation, Metallurgical Response and Behavior of Weld Fusion and HAZ in Cr-Mo Steels for Fossil Applications," Report No. ORNL/Sub/81-07685/02&77, Oak Ridge National Laboratory, Oak Ridge, TN.
9. B. Paulson: *Corr. Sci.*, 1978, vol. 18, p. 371.
10. M. Dewitte and C. Coussement: *Mater. High Temp.*, 1991, vol. 9, p. 178.
11. K. Laha, K.B.S. Rao, and S.L. Mannan: *Mater. Sci. Eng.*, 1990, vol. 129A, p. 183.
12. J.G. Zhang, F.W. Noble, and B.L. Eyre: *Mater. Sci. Eng.*, 1991, vol. 7, p. 315.
13. R.S. Fidler and D.J. Gooch: *Proc. Int. Conf. Ferritic Steels Fast Reactor Steam Generators*, S.F. Pugh and E.A. Little, eds., British Nuclear Energy Society, London, 1978, p. 128.
14. H.K.D.H. Bhadeshia, S.A. David, and J.M. Vitek: *Mater. Sci. Technol.*, 1991, vol. 7, p. 50.
15. G.S. Kim, J.E. Indacochea, and T.D. Spry: *Mater. Sci. Technol.*, 1991, vol. 7, p. 42.
16. C.K. Elliot, G.E. Lucas, R. Maiti, and G.R. Odette: *J. Nucl. Mater.*, 1986, vol. 141–143, p. 439.
17. R.K. Singh Raman and A.K. Tyagi: *Mater. Sci. Eng. A*, 1994, vol. 185, p. 97.
18. N. Parvathavarthini, R.K. Dayal, and J.B. Gnanamoorthy: *Corrosion*, 1996, vol. 52, p. 540.
19. O.P. Modi, M.N. Mungole, and K.P. Singh: *Corr. Sci.*, 1990, vol. 30, p. 941.
20. R.P. Singh, O.P. Modi, M.N. Mungole, and K.P. Singh: *Br. Corr. J.*, 1985, vol. 20, p. 28.
21. N. Parvathavarthini, R.K. Dayal, and J.B. Gnanamoorthy: *Bull. Electrochem.*, 1990, vol. 691, p. 20.
22. R.K. Singh Raman and J.B. Gnanamoorthy: *Welding J.*, 1995, vol. 74, p.133-s.
23. R.K. Singh Raman and J.B. Gnanamoorthy: *Corr. Sci.*, 1993, vol. 34, p. 1275.
24. K. Laha, K.S. Chandravathi, K.B.S. Rao, and S.L. Mannan: *Int. J. Pressure Vessel Piping*, 1995, vol. 62, p. 303.
25. S.J. Sanderson: *Proc. Int Conf. on Production, Fabrication, Properties and Applications of Ferritic Steels for High Temperature Applications*, Warrendale, PA, Oct. 1981, A.K. Khare, ed., ASM, Metals Park, OH, 1981, p. 85.
26. P. Patriarca, S.D. Harkness, J.M. Duke, and L.R. Cooper: *Nucl. Technol.*, 1976, vol. 28, p. 516.
27. S. Saroja, M. Vijayalakshmi, and V.S. Raghunathan: *Mater. Trans. Jpn. Inst. Met.*, 1993, vol. 34, p. 901.
28. M. Vijayalakshmi, S. Saroja, V. Thomas Paul, R. Mythili, and V.S. Raghunathan: *Metall. Trans. A*, 1999, vol. 30A, p. 161.
29. K. Laha: Ph.D. Desertation, Indian Institute of Science, Bangalore, 1998, p. 77.
30. D.R. Harries: *Proc. Conf. on Ferritic Alloys for Use in Nuclear Technology*, Snowbird, UT, J.W. Davis and D.J. Michael, eds., TMS-AIME, New York, NY, 1984, p. 141.
31. B. Buchamyr, H. Cerjak, M. Mitwer, and J. S. Kirkaldy: *Proc. Conf. on Recent Trends in Welding Science and Technology*, S.D. David and J.M. Vitek, eds., ASM International, Materials Park, OH, 1989, p. 291.
32. J.N. Soo: CEGB Report No. RD/L/R, CEGB, 1918.
33. F.B. Pickering and A.D. Vassiliou: *Met. Technol.*, 1980, vol. 7, p. 409.
34. S. Saroja, M. Vijayalakshmi, and V.S. Raghunathan: *J. Mater. Sci.*, 1992, vol. 27, p. 2389.
35. J.N. Soo: *Proc. Specialist Meeting on Mechanical Properties of Structural Materials Including Environmental Effects*, International Atomic Energy Agency (IAEA) and International Working Group on Fast Reactors (IWGFR), Chester, England, 1983, p. 579.
36. P.J. Alberry and W.K.C. Jones: *Met. Technol.*, 1977, vol. 4, p. 557.
37. S.N. Banerjee: *An Introduction to Science of Corrosion and Its Inhibition*, Oxonian Press Pvt. Ltd., New Delhi, p. 185.
38. H. Shaikh, G. George, F. Schneider, K. Mummert, and H.S. Khatak: *Proc. Int. Conf. on Emerging Trends in Corrosion Control—Evaluation, Monitoring and Solutions*, A.S. Khanna, K.S. Sharma, and A.K. Sinha, eds., Replica Press Pvt. Ltd., New Delhi, NACE International India Section, 1999, vol. I, p. 32.